European Journal of Chemistry

View Journal Online
View Article Online

Exploring the influence of ionic liquids on bimetallic gold nanoclusters and cellobiose through DFT analysis

Manohar Pillegowda [1], Susheela Krishnappa Lenkennavar [2] and Ganga Periyasamy [3,*]

[1] *Department of Chemistry, Nagarjuna College of Engineering and Technology, Bangalore, 562 164, India*
[2] *Department of Physics, Bangalore University, Bangalore, 560 056, India*
[3] *Department of Chemistry, Bangalore University, Bangalore, 560 056, India*

* *Corresponding author at: Department of Chemistry, Bangalore University, Bangalore, 560 056, India.*
e-mail: ganga.periyasamy@gmail.com (G. Periyasamy).

RESEARCH ARTICLE

10.5155/eurjchem.15.2.93-100.2486

Received: 25 October 2023
Received in revised form: 13 March 2024
Accepted: 8 April 2024
Published online: 30 June 2024
Printed: 30 June 2024

KEYWORDS

DFT
Ionic liquid
Gold cluster
Explicit solvation
Interface chemistry
Dilution of cellobiose

ABSTRACT

We conducted density functional theory (DFT) studies to investigate the potential cleavage of cellobiose into smaller fragments in an ecofriendly manner using bimetallic nanoclusters in an ionic liquid (IL) medium. The presence of IL solvent layers notably influences the behavior of gold clusters during the binding. Our study involves the simultaneous consideration of metal clusters and ILs to compute cellobiose structures. Our computational analysis reveals weak interactions between IL and cellobiose, whereas metal clusters exhibit robust binding to cellobiose via glycosidic oxygen. Introducing heterogeneity in metal clusters enhances their binding to cellobiose. Incorporation of hetero-metals induces polarization in the clusters, leading to dipole formation, as indicated by the electrostatic potential maps of halogenated clusters. Among the investigated clusters, those containing [Au_3Br(6IL)] exhibit notably strong binding to cellobiose, weakening the glycosidic bond by up to 7%. However, despite the strong interaction with metal clusters in an IL solvent, cleavage of the glycosidic bond remains elusive.

Cite this: *Eur. J. Chem.* **2024**, *15(2)*, 93-100 **Journal website**: www.eurjchem.com

1. Introduction

The depletion of fossil fuels and the global climate change have prompted researchers to shift their focus toward producing renewable chemicals and fuels from lignocellulosic biomass [1-3]. This plant material consists of cellulose, a linear polymer of glucose linked by β-1,4-glycosidic bonds, and a robust intra- and inter-molecular H-bonding network, constituting half of its weight [4,5]. Extensive efforts have been made to transform cellulose into valuable chemicals and biofuels, such as ethanol, 5-hydroxymethylfurfural, and levulinic acid, among others [6,7]. Furthermore, the materials derived from cellulose have wide applications as solvents, lubricants, and raw materials for fuel and chemical production [8,9]. However, achieving an environmentally friendly and economically viable conversion remains a challenge due to the poor solubility and conversion rate of the material [9-12].

To gain detailed knowledge and achieve optimal yields, researchers have individually addressed the dissolution and conversion processes [11,12]. Investigation into various solvents for dissolution has indicated the potential use of ionic liquid [13], recognized as a green solvent to dissolve cellulose at room temperature. Ionic liquids, characterized as molten salts, remain stable below ambient temperature, exhibit high chemical, thermal, and electrochemical stability, and offer practical attributes such as non-flammability and non-volatility [14-16]. Among the numerous ionic liquids, imidazole cations and acetate ions have been found to dissolve 15.0-20.5% of cellulose, 10% of hemicellulose, and 5% of lignin [17]. Oun and Rhim successfully extracted cellulose nanocrystals (CNCs) and cellulose nanofibers (CNFs) from seed fibers of *Calotropis procera* (Ushar) [18]. Computational and molecular dynamics studies have concluded that hydrogen bonding between acetate ions and cellulose is the reason for the solvation, a finding further supported by computed and measured spectroscopic parameters. To improve the solubility of cellulose, numerous methods have been proposed, including catalytic, bioenzymatic, and electrochemical approaches [19,20].

Catalytic methods offer significant advantages in conversion and dissolution, with the extensive use of nanoclusters in combination with ionic liquids [20]. Nanoclusters serve as catalysts in various conversion processes, including acting as oxidants, hydrogen catalysts, and biosensors for binding biomolecules (*e.g.*, lactate with Mn nanoparticles) [20-26].

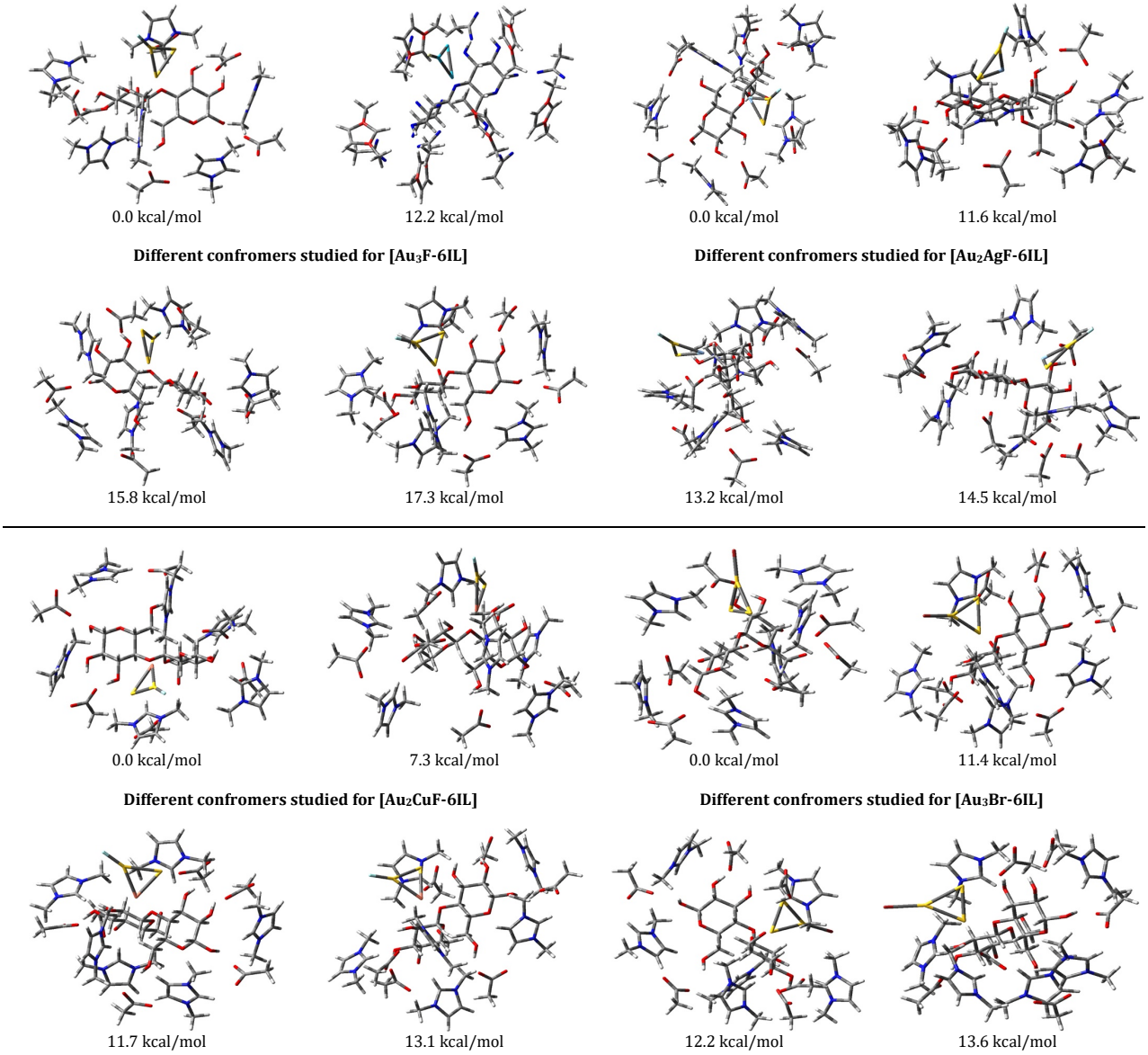

Figure 1. Different optimized conformers of the CB1-bound halogenated cluster with 6 pairs of ILs and the relative energies of the conformers.

Hybrid nanoclusters, which possess bifunctional characteristics, are particularly advantageous for cellulose conversion [27-30]. During the catalytic process, the protective ligand layer along with nanoclusters was demonstrated to play a crucial role. However, the specific chemical interactions of the ligands and the electrostatic interactions of the solvents are still unclear. This study aims to elucidate the potential binding modes of ionic liquids and nanoclusters with cellulose, using cellobiose as a model. To gain a deeper understanding, a heterogeneous ligation environment was created around the metal cluster. Additionally, the impact of the charge state was assessed by computing redox parameters, including donor and acceptor capacity.

2. Computational details

The metal clusters [Au_2M], [Au_2MX], where M = Au, Cu, and Ag, are optimized using the density functional theoretical method using the CAM-B3LYP hybrid functional with Grimme D2 dispersion correction as implemented in the Gaussian 09 package without any constraints. Los Alamos effective core potential (ECP) LANL2 with DZ basis set used for Au, Cu, and Ag. The lowest energy conformers of pure coinage metals (Au, Ag, and Cu) containing clusters exist in the singlet state.

In this work, 1,3-dimethylimidazolium acetate [$(C_1mim)^+(OAc)^-$] has been used as IL. The initial model for the metal cluster and ILs for the calculations is generated using the parameterized method 3 (PM3) semiempirical method. The optimized metal clusters are kept frozen in a position surrounded by 15 pairs of ILs in a random position. The optimization gives different structures for different sizes of clusters. In other words, the sizes of the PM3 optimized geometries are reduced to a uniform metal cluster-6IL environment and have been used as an initial guess for the DFT computations.

All DFT calculations reported in this work for IL media are performed using CAM-B3LYP hybrid functional with Grimme D2 dispersion correction as implemented in the Gaussian 09 package without any constraints [31,32]. Los Alamos effective core potential (ECP) LANL2 with DZ basis set used for Au, Cu, Ag and the 6-31+G(d,p) basis set for all other atoms, such as C, O, N, Cl, Br, and H atoms [33,34]. The convergence of forces with the options opt = tight (10^{-6} Hartree per bohr for the forces on atoms) and SCF = tight (10^{-8} Hartree convergence threshold).

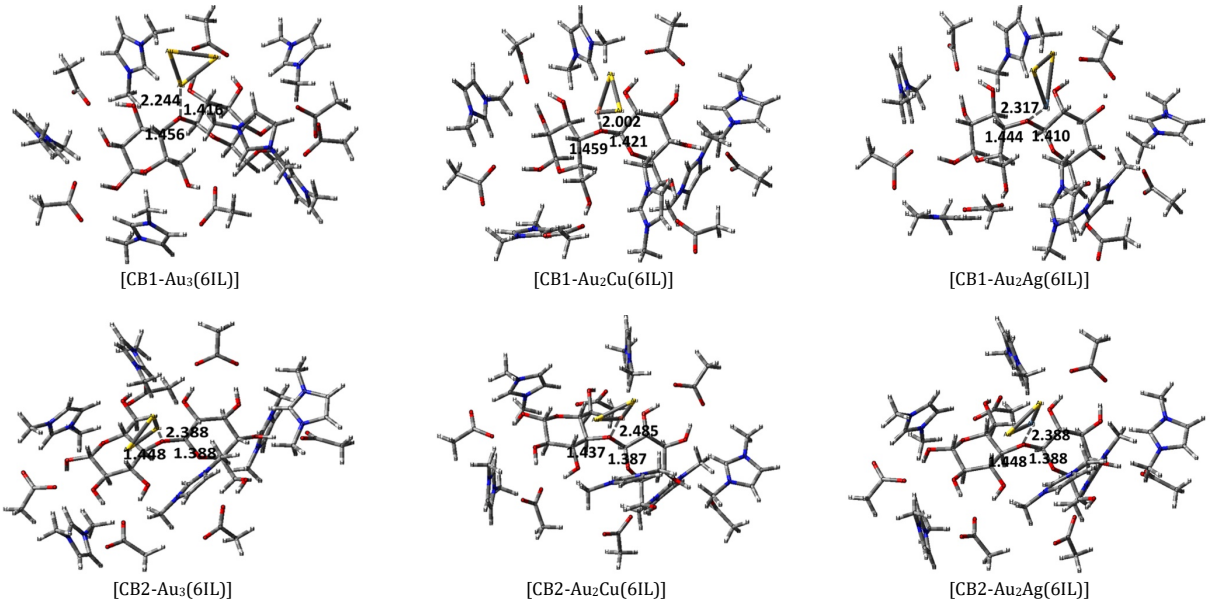

[CB1-Au$_3$(6IL)] [CB1-Au$_2$Cu(6IL)] [CB1-Au$_2$Ag(6IL)]

[CB2-Au$_3$(6IL)] [CB2-Au$_2$Cu(6IL)] [CB2-Au$_2$Ag(6IL)]

Figure 2. Computed structures of CB (anti-syn, anti-anti) with [Au$_2$M] clusters where M = Au, Cu and Ag. Important bond distances around glycosidic bonds are given in Å.

The presence of all real frequencies in harmonic vibrational calculations confirms the optimized geometry as minima in the PES. The calculation results in more than one possible conformer within 20 kcal/mol energy (as shown in Figure 1 for the halogenated cluster). The lowest energy structure was used for further analysis.

The Mulliken population analysis method is used to analyze the distribution of charge of the molecule. Mulliken charges are reported as average values for the metal cluster. The redox properties and donor-acceptors properties are calculated using Equations 1-4. The electron donor and electron acceptor indexes are calculated according to Gazquez and Vela [35] and defined as

$$\omega^{-}=\frac{(3\times \mathrm{VIE}+\mathrm{VEA})^2}{16\times(\mathrm{VIE}-\mathrm{VEA})} \quad (1)$$

$$\omega^{+}=\frac{(\mathrm{VIE}+3\times \mathrm{VEA})^2}{16\times(\mathrm{VIE}-\mathrm{VEA})} \quad (2)$$

$$\mathrm{VIE} = E_{\text{Cation sys. in neutral geo.}} - E_{\text{Neutral sys.}} \quad (3)$$

and

$$\mathrm{VEA} = E_{\text{Anion sys.in neutral geo.}} - E_{\text{Neutral sys.}} \quad (4)$$

VIE and VEA are calculated as the energy difference between the vertical states, which represents the vertical ionization energy and electron affinity, respectively. where ω- electron donating power and ω+ electron accepting power measure the propensity to donate and accept charge [36,37]. Donor-acceptor maps can predict reactivity by highlighting regions prone to nucleophilic or electrophilic attack, as they derive from VIE and VEA. This aids in rationalizing reaction mechanisms and designing new molecules with the desired reactivity profiles.

Metal with IL binding energy (E_b) is calculated using Equation 5.

$$E_b = E_{\text{Complex}} - (E_{M'_mM_nX} + 6 \times E_{IL}) \quad (5)$$

where E_{Complex}, $E_{M'_mM_nX}$ and E_{IL} are the total basis set superposition error corrected electronic energies of the neutral M'$_m$M$_n$X-6IL cluster, bare (M'$_m$M$_n$) and ionic liquid pair, respectively, where, M = Au, Cu and Ag. And the basis set superposition errors (BSSE) in binding energy values are calibrated using the Boys and Bernardi counterpoise correction method implemented in the Gaussian 09 package at the same level of theory [25].

3. Results and discussion

Cellobiose (CB) serves as a fundamental building block of cellulose, with D-glucose units linked to each other through beta linkages [38,39]. CB exhibits two conformers, anti-syn CB1 and anti-anti-CB2, with their stability order determined by the surrounding environment [40]. In the gas phase, anti-anti is the stable conformer, while in ionic liquid (IL) media, anti-syn is found to be the lowest energy state. Hence, both conformers are considered in this study. To mimic metal clusters, we used a previously established model [Au$_2$M] [38], with M representing Cu, Ag, and Au. Furthermore, the solvent environment is explicitly represented by the *N*,*N*-dimethyl imidazole cation and acetate anion IL pairs. DAM analysis shows that CB and CB-6IL are good electron donors with comparatively lower ω- value and metal clusters are good electron acceptor with higher ω- value.

3.1. Interaction between CB and [Au$_3$-6IL]^0 cluster

The computations reveal that the presence of various metal clusters and explicit IL pairs influences the energetics of the conformer CB1/CB2, depending on the nature of the metal cluster. In the case of [Au$_3$], the energy remains consistent with [CB-6IL], where the anti-syn (CB1) conformer is more stable than the anti-anti (CB2) conformer by 7.00 kcal/mol [40]. This stability is attributed to the intramolecular H-bonding interaction between IL and CB (Table 1 and Figure 2). Furthermore, the presence of the metal cluster increases the H-bond distance between IL-CB1 by approximately 0.1 Å. However, the binding energy value of CB1-[Au$_3$(6IL)] (26 kcal/mol) is higher than that of CB1-6IL (21 kcal/mol), attributed to the charge transfer from CB to the metal cluster, as indicated by the Mulliken charge analysis (Table 2).

Table 1. The computed energy difference between CB1/CB2-metal clusters, binding energy (E_b), the bond distances of the clusters in Å.

Molecules	ΔE = CB1-CB2 (kcal/mol)	E_b (kcal/mol)	Number of H-bonds with acetate/imidazole	H-O distance of CB unit interacting with IL $(C_1mim)^+$	O-H distance of CB unit interacting with IL $(OAc)^-$	M-O
[CB1-Au_3(6IL)]	-3.63	-354.20	12/7	2.329	2.054	2.244
[CB2-Au_3(6IL)]		-316.21	10/9	2.322	1.878	2.388
[CB1-Au_2Cu(6IL)]	-10.90	-314.54	12/8	2.402	2.068	2.002
[CB2-Au_2Cu(6IL)]		-317.36	10/9	2.117	1.881	2.485
[CB1-Au_2Ag(6IL)]	-10.47	-311.25	12/9	2.498	2.067	2.317
[CB2-Au_2Ag(6IL)]		-307.51	10/9	2.438	1.878	2.388

Table 2. Computed bond distances (Å) and Mulliken charges (e) of neutral clusters.

Molecules	Glycosidic C-O	Glyclosidic O-C	Mulliken charge, e		
			Metal cluster	CB	IL
[CB1-Au_3]	1.450	1.400	-0.2710	0.2710	-
[CB2-Au_3]	1.450	1.403	-0.2170	0.2170	-
[CB1-Au_3(6IL)]	1.456	1.416	-0.2923	-0.1597	0.8579
[CB2-Au_3(6IL)]	1.448	1.388	-0.9231	-1.1102	1.2485
[CB1-Au_2Cu(6IL)]	1.459	1.421	-0.2848	-0.4300	0.7147
[CB2-Au_2Cu(6IL)]	1.437	1.387	-0.2848	-1.2535	1.5383
[CB1-Au_2Ag(6IL)]	1.444	1.410	-0.3098	-0.4175	0.7272
[CB2-Au_2Ag(6IL)]	1.448	1.388	-0.4312	-1.1905	1.6216

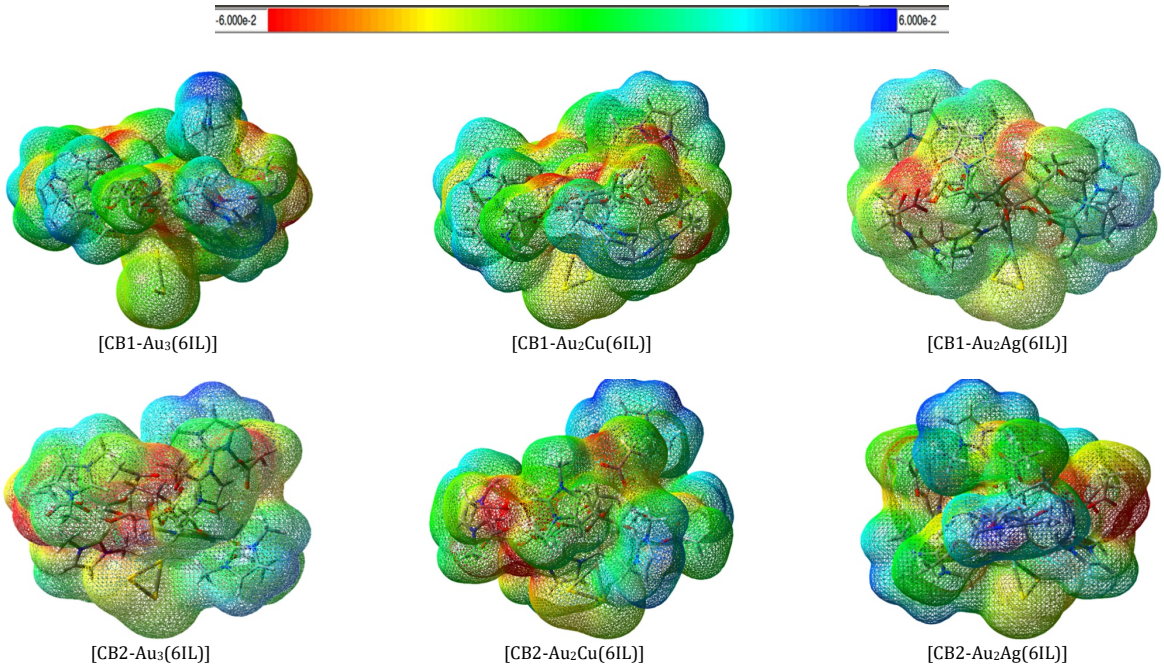

Figure 3. Molecular electrostatic potential (ESP) map of CB1/CB2-metal clusters with isocontour value of 0.004 $Å^{-3}$.

The larger negative charge at the metal cluster (in e) in the CB1-[Au_3(6IL)] system provides evidence of the charge transfer nature, with the metal cluster acting as an electron acceptor. This is supported by DAM analysis, which shows an enhancement in the cluster's donation ability in the presence of the IL layer with lower ω-. Consequently, the hydrogen bond distance between the NH group of the imidazole cation in IL and the O of CB is reduced by 2.329 Å. Furthermore, the bond distance between the O of the acetate ion and the H atom of CB decreases in the presence of IL media (Tables 1 and 2). The bond distance between the glycosidic bond C1-O4 increases by 0.06-0.10 Å, but both glucose units remain intact. Since population analysis underscores the importance of the charge transfer nature, heterogeneity is introduced by employing bimetallic clusters and a ligation environment to enhance polarization at the metal cluster.

3.2. Interaction between CB and [Au_2M-6IL]^0 cluster

A significant amount of charge transfer (CT) affects the glycosidic bond, prompting the introduction of heterogeneity within the cluster in the hope of breaking the C-O linkage of the glycosidic bond. To maintain the cluster size, we incorporate coinage metals as bimetallic components. The bimetallic component decreases the binding capacity due to this heterogeneity, as reflected in the order of the M-O bond lengths: [CB-Au_3(6IL)] < [CB-Au_2Ag(6IL)] < [CB-Au_2Cu(6IL)] (Table 3).

The presence of heterogeneity does not alter the conformer stability. However, the energy difference between the conformers increases due to the higher stabilization of the CB1-Au_2M-6IL conformer (by -10 kcal/mol) with a greater number of H-bonding interactions compared to CB2-Au_2M-6IL. Among these three clusters, the copper-containing cluster more effectively weakens the glycosidic linkage than the other clusters, attributed to its higher electron-accepting capacity, as reflected in DAM map analysis. The polarizability of all three clusters increases, as depicted in the electrostatic potential map in Figure 3. Furthermore, the computed HOMO-LUMO gap indicates their enhanced chemical stability.

To further enhance the influence of the glycosidic bond, the oxidation state of the cluster is tuned, as experimental analysis suggests the metal cluster's role as an oxidant. The oxidation state is adjusted by introducing halogen coordination around the metal cluster.

Table 3. Computed bond distances (Å) and Mulliken charges (e) of cationic clusters.

Molecules	C-O	O-C	M-O	Mulliken charge (e)		
				Metal cluster	CB	IL
[CB1-Au_3(6IL)]	1.437	1.396	3.105	0.5211	-0.2992	0.7780
[CB2-Au_3(6IL)]	1.465	1.459	2.228	0.4466	-1.0943	1.6477
[CB1-Au_2Cu(6IL)]	1.451	1.399	2.514	0.5181	-0.3357	0.8178
[CB2-Au_2Cu(6IL)]	1.459	1.418	2.296	0.3732	-1.1795	1.8063
[CB1-Au_2Ag(6IL)]	1.446	1.401	2.432	0.5074	-0.3303	0.8229
[CB2-Au_2Ag(6IL)]	1.465	1.416	2.199	0.2965	-1.1215	1.8349

Table 4. Bond angle (°) and bond distance (Å) of CB that interacts with $[Au_2M(6IL)]^+ X^-$ clusters, where X = F, Cl, and Br.

Clusters	$d_{M\text{-}Oglycosdic}$	$d_{M\text{-}O*glycosdic}$	$d_{C\text{-}Oglycosdic}$	$d_{O\text{-}Cglycosdic}$	< C-O-C $_{glycosdic}$
CB-[Au_3F((6IL))]	2.573	2.267	1.433	1.394	120
CB-[Au_3Br(6IL)]	3.404	3.031	1.454	1.399	118
CB-[Au_2CuF(6IL)]	2.765	3.468	1.415	1.391	115
CB-[Au_2CuBr(6IL)]	2.183	2.232	1.442	1.411	119
CB-[Au_2AgF(6IL)]	2.360	2.856	1.433	1.419	118
CB-[Au_2AgBr(6IL)]	3.735	3.734	1.437	1.409	106

Table 5. Mulliken charges (e) of CB interacting with $[Au_2M(6IL)]^+ X^-$ clusters, where X = F, Cl, and Br.

Clusters	CB	Metal	X
CB-[Au_3F(6IL)]	-0.362	0.417	-0.576
CB-[Au_3Br(6IL)]	-0.332	0.116	-0.257
CB-[Au_2CuF(6IL)]	-0.538	-0.343	0.627
CB-[Au_2CuBr(6IL)]	-0.472	0.231	-0.622
CB-[Au_2AgF(6IL)]	-0.497	0.545	-0.580
CB-[Au_2AgBr(6IL)]	-0.550	-0.159	-0.219

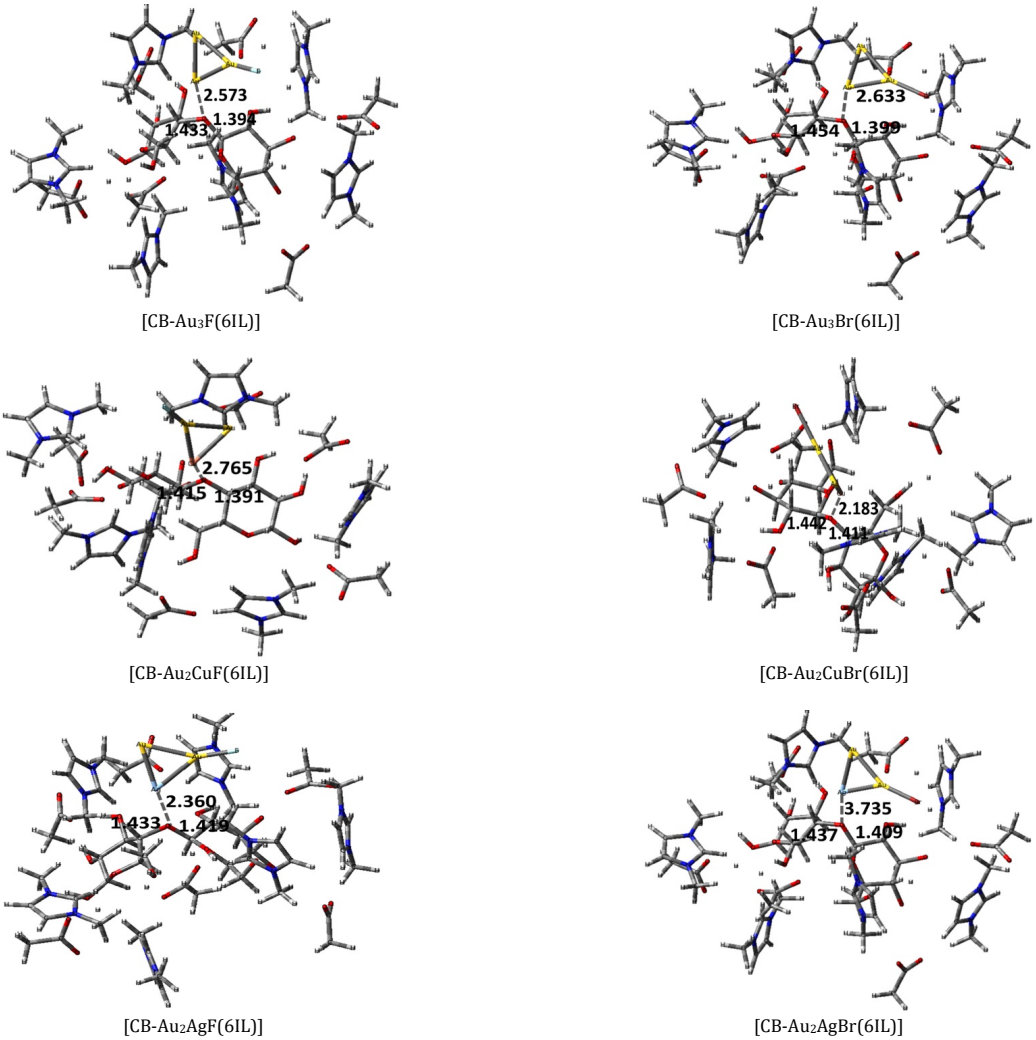

[CB-Au_3F(6IL)] [CB-Au_3Br(6IL)]

[CB-Au_2CuF(6IL)] [CB-Au_2CuBr(6IL)]

[CB-Au_2AgF(6IL)] [CB-Au_2AgBr(6IL)]

Figure 4. Anti-syn CB interacting with $[Au_2M(6IL)]^+ X^-$ clusters. Important bond distances around glycosidic bonds are given in Å.

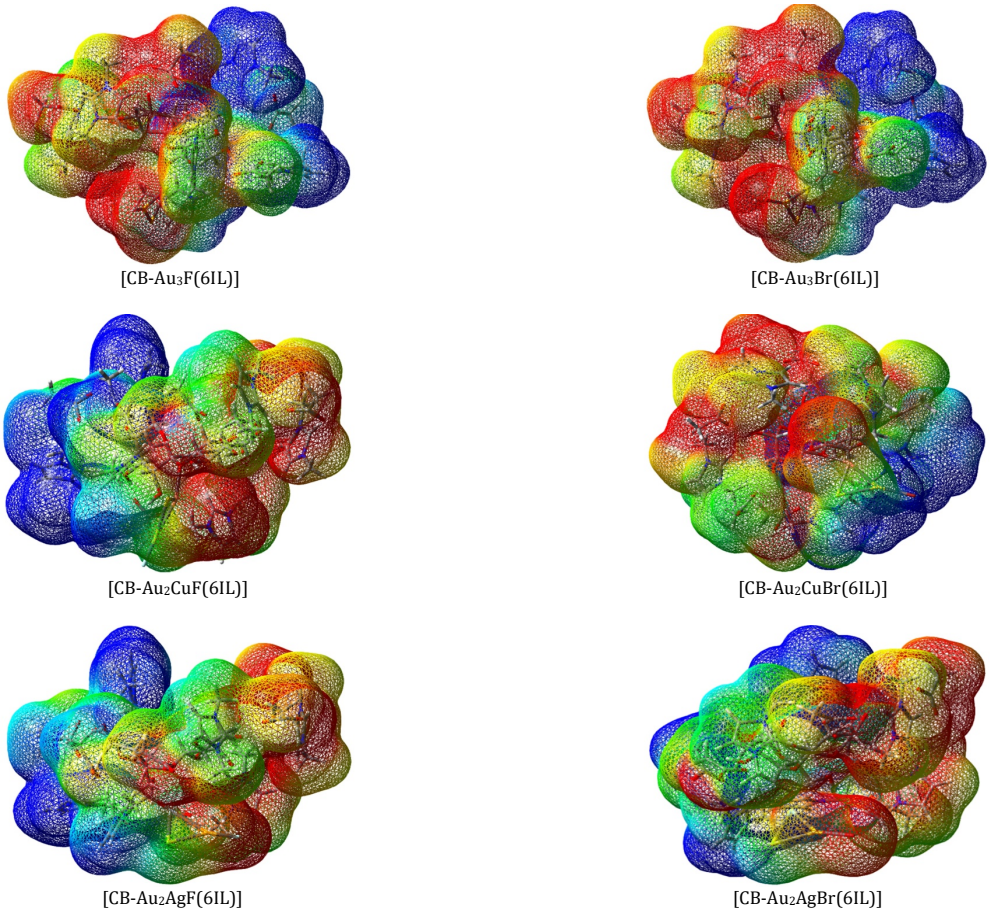

Figure 5. Molecular electrostatic potential (ESP) map of CB1/CB2-[$Au_2M(6IL)X$] metal clusters with isocontour value of 0.004 $Å^{-3}$.

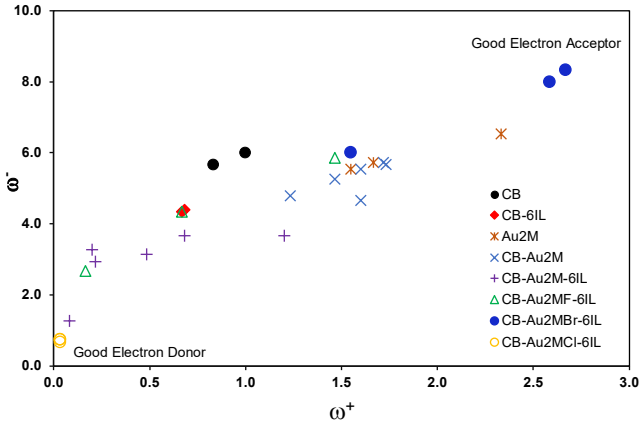

Figure 6. The donor acceptor map is calculated using the equation given in the computational section.

3.3. Interaction between CB and [$Au_2M(6IL)]^+ X^-$ cluster

In our previous research [38,40], we have demonstrated that the halogenation of the metal cluster exhibits an increased interaction efficiency in the gas phase, a characteristic that has been confirmed to persist within the solvent layer. Furthermore, it should be noted that the halogen atom is observed to form hydrogen bonds with the IL layer, as illustrated in Figure 4. The charge separation is apparent from the ESP map of the halogenated cluster in Figure 5, which shows the repulsion between the two units (Table 4). Detailed analysis, including the donor acceptor map (Figure 6) and Mulliken population evaluation (Table 5), indicates an improved acceptor efficiency with larger ω^+ values for chlorine (Cl)-containing clusters, while bromine (Br) and fluorine (F) containing clusters exhibit efficiency similar to that of bare clusters.

4. Conclusions

The influence of IL solvation on the glycosidic bond cleavage in the presence of bimetallic clusters has been explored in this work. The computations on the same are found to predict that the electron-donating and accepting abilities of the respective metal clusters and cellobiose got enhanced in the presence of solvent environment. These interactions make the glycosidic bond more vulnerable towards cleavage. Computed ESP plots provide evidence for the polarizability induced by the halogen atoms in the cluster. Among the clusters studied here,

CB-[Au_3Br(6IL)] was found to cause the glycosidic bond to be distorted to a greater extent. Both cellobiose conformers were found to follow a similar trend in being susceptible to cleavage on interaction with the metal cluster. However, the interaction with metal clusters in an IL solvation is not enough for the glycosidic bond breakdown.

Acknowledgements

This study was supported by the University Grant Commission Faculty Recharge Program/(UGC-FRP(2013) Basic Scientific Research for funding and Vision group on science and technologies (VGST-KFIST-L2/GRD-1021/118/2022-23/94).

Disclosure statement

Conflict of interest: The authors declare that they have no conflict of interest. Ethical approval: All ethical guidelines have been followed.

CRediT authorship contribution statement

Conceptualization: Ganga Periyasamy; Methodology: Ganga Periyasamy, Manohar Pillegowda; Software: Ganga Periyasamy; Validation: Ganga Periyasamy, Manohar Pillegowda, Susheela Krishnappa Lenkennavar; Formal Analysis: Ganga Periyasamy, Manohar Pillegowda, Susheela Krishnappa Lenkennavar; Investigation: Ganga Periyasamy, Manohar Pillegowda, Susheela Krishnappa Lenkennavar; Resources: Ganga Periyasamy, Manohar Pillegowda, Susheela Krishnappa Lenkennavar; Data Curation: Ganga Periyasamy, Manohar Pillegowda, Susheela Krishnappa Lenkennavar; Writing - Original Draft: Ganga Periyasamy, Manohar Pillegowda, Susheela Krishnappa Lenkennavar; Writing - Review and Editing: Ganga Periyasamy, Manohar Pillegowda, Susheela Krishnappa Lenkennavar; Visualization: Ganga Periyasamy, Manohar Pillegowda, Susheela Krishnappa Lenkennavar; Funding acquisition: Ganga Periyasamy; Supervision: Ganga Periyasamy; Project Administration: Ganga Periyasamy.

ORCID and Email

Manohar Pillegowda
manohargowda888@gmail.com
https://orcid.org/0009-0004-6047-2699
Susheela Krishnappa Lenkennavar
sushhh10@gmail.com
https://orcid.org/0000-0002-5068-0564
Ganga Periyasamy
ganga.periyasamy@gmail.com
https://orcid.org/0000-0002-8675-5935

References

[1]. Limayem, A.; Ricke, S. C. Lignocellulosic biomass for bioethanol production: Current perspectives, potential issues and future prospects. *Prog. Energy Combust. Sci.* **2012**, *38*, 449–467.
[2]. Climent, M. J.; Corma, A.; Iborra, S. Converting carbohydrates to bulk chemicals and fine chemicals over heterogeneous catalysts. *Green Chem.* **2011**, *13*, 520.
[3]. Mandels, M.; Reese, E. T. Induction of cellulase in fungi by cellobiose. *J. Bacteriol.* **1960**, *79*, 816–826.
[4]. Conley, K.; Godbout, L.; Whitehead, M. A. (tony); van de Ven, T. G. M. Origin of the twist of cellulosic materials. *Carbohydr. Polym.* **2016**, *135*, 285–299.
[5]. Takagaki, A.; Nishimura, S.; Ebitani, K. Catalytic transformations of biomass-derived materials into value-added chemicals. *Catal. Surv. Asia* **2012**, *16*, 164–182.
[6]. Huber, G. W.; Iborra, S.; Corma, A. Synthesis of transportation fuels from biomass: Chemistry, catalysts, and engineering. *Chem. Rev.* **2006**, *106*, 4044–4098.
[7]. Henriksson, G.; Salumets, A.; Divne, C.; Pettersson, G. Studies of cellulose binding by cellobiose dehydrogenase and a comparison with cellobiohydrolase 1. *Biochem. J.* **1997**, *324*, 833–838.
[8]. Toshima, N.; Yonezawa, T. Bimetallic nanoparticles—novel materials for chemical and physical applications. *New J Chem* **1998**, *22*, 1179–1201.
[9]. Binder, J. B.; Raines, R. T. Fermentable sugars by chemical hydrolysis of biomass. *Proc. Natl. Acad. Sci. U. S. A.* **2010**, *107*, 4516–4521.
[10]. Wang, A.; Zhang, T. One-pot conversion of cellulose to ethylene glycol with multifunctional tungsten-based catalysts. *Acc. Chem. Res.* **2013**, *46*, 1377–1386.
[11]. Kaufman Rechulski, M. D.; Käldström, M.; Richter, U.; Schüth, F.; Rinaldi, R. Mechanocatalytic depolymerization of lignocellulose performed on hectogram and kilogram scales. *Ind. Eng. Chem. Res.* **2015**, *54*, 4581–4592.
[12]. Qian, X.; Nimlos, M. R.; Davis, M.; Johnson, D. K.; Himmel, M. E. Ab initio molecular dynamics simulations of β-d-glucose and β-d-xylose degradation mechanisms in acidic aqueous solution. *Carbohydr. Res.* **2005**, *340*, 2319–2327.
[13]. Zhang, Y.; Cui, X.; Shi, F.; Deng, Y. Nano-gold catalysis in fine chemical synthesis. *Chem. Rev.* **2012**, *112*, 2467–2505.
[14]. An, D.; Ye, A.; Deng, W.; Zhang, Q.; Wang, Y. Selective conversion of cellobiose and cellulose into gluconic acid in water in the presence of oxygen, catalyzed by polyoxometalate-supported gold nanoparticles. *Chemistry* **2012**, *18*, 2938–2947.
[15]. Sarkar, N.; Ghosh, S. K.; Bannerjee, S.; Aikat, K. Bioethanol production from agricultural wastes: An overview. *Renew. Energy* **2012**, *37*, 19–27.
[16]. Nigam, P. S.; Singh, A. Production of liquid biofuels from renewable resources. *Prog. Energy Combust. Sci.* **2011**, *37*, 52–68.
[17]. Zhang, Q.; Zhang, S.; Deng, Y. Recent advances in ionic liquid catalysis. *Green Chem.* **2011**, *13*, 2619.
[18]. Wang, A.-Q.; Chang, C.-M.; Mou, C.-Y. Evolution of catalytic activity of Au–Ag bimetallic nanoparticles on mesoporous support for CO oxidation. *J. Phys. Chem. B* **2005**, *109*, 18860–18867.
[19]. Baishya, S.; Deka, R. C. Catalytic Activities of Au6, , and Clusters for CO oxidation: A density functional study. *Int. J. Quantum Chem.* **2014**, *114*, 1559–1566.
[20]. Yan, N.; Zhao, C.; Luo, C.; Dyson, P. J.; Liu, H.; Kou, Y. One-step conversion of cellobiose to C6-alcohols using a ruthenium nanocluster catalyst. *J. Am. Chem. Soc.* **2006**, *128*, 8714–8715.
[21]. Hayashi, N.; Sakai, Y.; Tsunoyama, H.; Nakajima, A. Development of ultrafine multichannel microfluidic mixer for synthesis of bimetallic nanoclusters: Catalytic application of highly monodisperse AuPd nanoclusters stabilized by poly(*N*-vinylpyrrolidone). *Langmuir* **2014**, *30*, 10539–10547.
[22]. Welton, T. Room-temperature ionic liquids. Solvents for synthesis and catalysis. *Chem. Rev.* **1999**, *99*, 2071–2084.
[23]. Gao, M.-R.; Yuan, J.; Antonietti, M. Frontispiece: Ionic liquids and poly(ionic liquid)s for morphosynthesis of inorganic materials. *Chemistry* **2017**, *23*.
[24]. Feng, J.-J.; Lin, X.-X.; Chen, L.-X.; Liu, M.-T.; Yuan, J.; Wang, A.-J. Ionic liquid-assisted synthesis of composition-tunable cross-linked AgPt aerogels with enhanced electrocatalysis. *J. Colloid Interface Sci.* **2017**, *498*, 22–30.
[25]. Itoh, H.; Naka, K.; Chujo, Y. Synthesis of gold nanoparticles modified with ionic liquid based on the imidazolium cation. *J. Am. Chem. Soc.* **2004**, *126*, 3026–3027.
[26]. Kudo, S.; Zhou, Z.; Yamasaki, K.; Norinaga, K.; Hayashi, J.-I. Sulfonate ionic liquid as a stable and active catalyst for levoglucosenone production from saccharides via catalytic pyrolysis. *Catalysts* **2013**, *3*, 757–773.
[27]. Jameel, U.; Zhu, M.; Chen, X.; Tong, Z. Recent progress of synthesis and applications in polyoxometalate and nanogold hybrid materials. *J. Mater. Sci.* **2016**, *51*, 2181–2198.
[28]. Corma, A.; Garcia, H. Supported gold nanoparticles as catalysts for organic reactions. *Chem. Soc. Rev.* **2008**, *37*, 2096.
[29]. Tokonami, S.; Morita, N.; Takasaki, K.; Toshima, N. Novel synthesis, structure, and oxidation catalysis of Ag/Au bimetallic nanoparticles. *J. Phys. Chem. C Nanomater. Interfaces* **2010**, *114*, 10336–10341.
[30]. Pei, Y.; Tang, J.; Tang, X.; Huang, Y.; Zeng, X. C. New structure model of Au22(SR)18: Bitetrahederon golden kernel enclosed by [Au6(SR)6] Au(I) complex. *J. Phys. Chem. Lett.* **2015**, *6*, 1390–1395.
[31]. Yanai, T.; Tew, D. P.; Handy, N. C. A new hybrid exchange–correlation functional using the Coulomb-attenuating method (CAM-B3LYP). *Chem. Phys. Lett.* **2004**, *393*, 51–57.
[32]. Frisch, M. J.; Trucks, G. W.; Schlegel, H. B.; Scuseria, G. E.; Robb, M. A.; Cheeseman, J. R.; Montgomery, J. A.; Vreven, T.; Kudin, K. N.; Burant, J. C.; Millam, J. M.; Iyengar, S. S.; Tomasi, J.; Barone, V.; Mennucci, B.; Cossi, M.; Scalmani, G.; Rega, N.; Petersson, G. A.; Nakatsuji, H.; Hada, M.; Ehara, M.; Toyota, K.; Fukuda, R.; Hasegawa, J.; Ishida, M.; Nakajima, T.; Honda, Y.; Kitao, O.; Nakai, H.; Klene, M.; Li, X.; Knox, J. E.; Hratchian, H. P.; Cross, J. B.; Adamo, C.; Jaramillo, J.; Gomperts, R.; Stratmann, R. E.; Yazyev, O.; Austin, A. J.; Cammi, R.; Pomelli, C.; Ochterski, J. W.; Ayala, P. Y.; Morokuma, K.; Voth, G. A.; Salvador, P.; Dannenberg, J. J.; Zakrzewski, V. G.; Dapprich, S.; Daniels, A. D.; Strain, M. C.; Farkas, O.; Malick, D. K.; Rabuck, A. D.; Raghavachari, K; Foresman, J. B.; Ortiz, J. V.; Cui, Q.; Baboul, A. G.; Clifford, S.; Cioslowski, J.; Stefanov, B. B.; Liu, G.; Liashenko, A.; Piskorz, P.; Komaromi, I.; Martin, R. L.; Fox, D. J.; Keith, T.; Al-Laham, M. A.; Peng, C. Y.; Nanayakkara, A.; Challacombe, M.; Gill, P. M. W.; Johnson, B.; Chen, W.; Wong, M. W.; Gonzalez, C.; Pople, J. A. Gaussian 09 Revision E.01, Gaussian, Inc., Wallingford CT, 2004.
[33]. Tlahuice-Flores, A.; Whetten, R. L.; Jose-Yacaman, M. Vibrational normal modes of small thiolate-protected gold clusters. *J. Phys. Chem. C Nanomater. Interfaces* **2013**, *117*, 12191–12198.

[34]. Boys, S. F.; Bernardi, F. The calculation of small molecular interactions by the differences of separate total energies. Some procedures with reduced errors. *Mol. Phys.* **1970**, *19*, 553–566.
[35]. Gázquez, J. L.; Cedillo, A.; Vela, A. Electrodonating and electroaccepting powers. *J. Phys. Chem. A* **2007**, *111*, 1966–1970.
[36]. Martínez, A.; Rodríguez-Gironés, M. A.; Barbosa, A.; Costas, M. Donator acceptor map for carotenoids, melatonin and vitamins. *J. Phys. Chem. A* **2008**, *112*, 9037–9042.
[37]. Martínez, A. Gold–bismuth clusters. *J. Phys. Chem. A* **2014**, *118*, 5894–5902.
[38]. Pillegowda, M.; Periyasamy, G. DFT studies on interaction between bimetallic [Au 2 M] clusters and cellobiose. *Comput. Theor. Chem.* **2018**, *1129*, 26–36.
[39]. Su, J.; Qiu, M.; Shen, F.; Qi, X. Efficient hydrolysis of cellulose to glucose in water by agricultural residue-derived solid acid catalyst. *Cellulose* **2018**, *25*, 17–22.
[40]. Payal, R. S.; Bharath, R.; Periyasamy, G.; Balasubramanian, S. Density functional theory investigations on the structure and dissolution mechanisms for cellobiose and Xylan in an ionic liquid: Gas phase and cluster calculations. *J. Phys. Chem. B* **2012**, *116*, 833–840.